PHYSICAL REVIEW A VOLUME 26, NUMBER 6 DECEMBER 1982

Breather annihilation by simple dissipation

D. W. McLaughlin
Department of Mathematics and Program in Applied Mathematics, University of Arizona, Tucson, Arizona 85704

E. A. Overman II
Department of Mathematics and Statistics, University of Pittsburgh, Pittsburgh, Pennsylvania 15261

(Received 21 October 1981)

A numerical experiment is conducted on the decay of a sine-Gordon breather under simple dissipation. Both the spatial configuration and the (nonlinear) spectral configurations are measured numerically. The spectral configuration establishes that the breather is annihilated in finite time and that the annihilation process is accomplished by the generation of a long-wavelength packet of dispersive radiation. The nonlinear radiation density, which is measured numerically, is seen to be order 1 and is extremely well approximated by a sech profile in k space. Finally, a representation of the spectral configuration by "resonance" states is investigated.

I. INTRODUCTION

Processes which change the number of solitons in a nonlinear wave (either through annihilation or creation) are not well understood. These processes proceed by conversions between collective soliton modes and radiation modes; unfortunately, radiation modes are difficult to describe analytically.

In this paper we describe one simple numerical experiment in which a soliton is destroyed—the annihilation of a sine-Gordon breather by dissipation. Primarily, we chose this experiment because its simplicity should permit an analytical description. The experiment would then provide insight and numerical facts for such a description. In addition, it is related to a fundamental problem in the statistical mechanics of nonlinear Klein-Gordon fields, namely, should *both* breathers and radiation be treated as fundamental excitations[1,2] in a statistical description of the field.

In Sec. III we describe a numerical experiment which measures both the spatial and spectral representations of the wave at different times during the annihilation process. Although equivalent, these two representations provide complementary information. In particular, the spectral representation provides a *direct numerical* measurement of the number and type of solitons and the density of *nonlinear* radiation which comprises the wave at time t. For example, the spectral representation provides a precise mathematical rule which determines the presence or absence of solitons in the wave. In addition, most analyses of solitons under perturbations[3–5] work directly with the spectral representation. Our numerical experiment, in contrast with most other numerical calculations, measures directly the (nonlinear) spectral representation.

The numerical experiment demonstrates the actual annihilation of the breather in finite time (as opposed to a gradual relaxation to zero amplitude). The numerical measurement of the nonlinear radiation density shows that long-wavelength radiation becomes an order 1 [as opposed to $O(\epsilon)$] effect during times near the annihilation time. The measurement depicts the actual k-space profile of the radiation density at different times. These measurements indicate that the annihilation process occurs by the breather state transferring into radiation, which is then lost to dissipation.

In Sec. IV we analyze the spectral numerical data. We are motivated by a desire to characterize the radiation modes which participate in the annihilation process in terms of a few (physical) parameters, just as solitons are characterized by their location and velocity. We show, for all calculated values of time, the radiation density is extremely well approximated by a sech profile in k space. This sech profile seems very suggestive for an analytical representation of the radiation. Then we consider a second possibility, a rational-function approximation to the radiation profiles. This approximation would characterize the radiation in terms of poles of the spectral representation in the lower half plane ("resonances") just as solitons are characterized by poles of the spectral representa-

tion in the upper half plane ("eigenvalues"). This approach is certainly consistent with our numerical data, which shows breather annihilation occurs by the motion of the breather poles across the real axis into the lower half plane. In Sec. IV we find that such a resonance approximation can be accurate and then we study the motion of the leading resonances during the annihilation process.

Our studies indicate that either the sech profile or the resonances could provide accurate descriptions of the radiation, which depends upon a few parameters and thus are candidates for low-dimensional representations of the radiation packets which participate in the annihilation process. In addition to stimulating analysis of the annihilation of solitons, this simple experiment illustrates the useful information that can be obtained by a numerical evaluation of the nonlinear spectral representation. We believe this representation should be used more frequently to display the results of numerical experiments of perturbed soliton equations.

II. PRELIMINARIES

The sine-Gordon equation

$$u_{tt}-u_{xx}+\sin u=0\ , \tag{2.1}$$

admits a "breather" solution which, when at rest in the laboratory frame, is given by

$$u^{(B)}(x,t;\nu)\equiv \tanh^{-1}\times\left[\frac{\tan\nu\cos[(\cos\nu)t]}{\cosh[(\sin\nu)x]}\right]\ . \tag{2.2}$$

Such a breather is sketched in Fig. 1 for $\nu=20°$, which is the initial condition to be used in the remainder of this paper. Notice it is a solitary (particlelike) wave which breathes periodically in time. The parameter ν fixes the frequency of the breather ($\cos\nu$) and its amplitude (4ν). The spatial

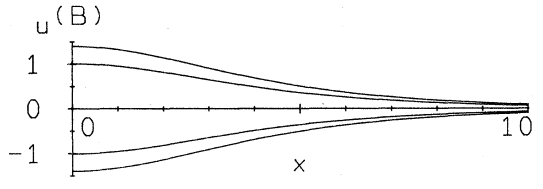

FIG. 1. Pure breather solution, Eq. (2.2) with $\nu=20°$, at times $t=m\pi/(4\cos 20°)$ for $m=0$ (top curve), 1, 2 (x axis), 3, and 4 (bottom curve).

width is parametrized by $1/\sin\nu$ and its energy is $16\sin\nu$.

As the parameter ν goes to zero,

$$u^{(B)}\simeq 4\nu\,\mathrm{sech}(\nu x)\cos\left[\left[1-\frac{\nu^2}{2}\right]t\right]\ ;$$

thus, as $\nu\to 0$, the amplitude and energy decrease to zero, the frequency increases to 1, while the temporal period decreases to 2π. Moreover, the spatial extent of the wave increases. These characteristics should be contrasted with those of near-linear radiation states. In particular, the linear dispersion relation $\omega^2(\kappa)=1+\kappa^2$ shows that only long-wavelength ($\kappa\simeq 0$ or "plasma") radiation has a frequency near 1. Thus under perturbations, small-amplitude breathers should resonate with long-wavelength plasma radiation.

Next, we consider the addition of simple dissipation

$$u_{tt}-u_{xx}+\sin u=-\epsilon u_t\ , \qquad t>0,\ 0<\epsilon<<1 \tag{2.3}$$

with breather initial conditions,

$$u(x,t)=u^{(B)}(x,t),\quad t<0\ . \tag{2.4}$$

This dissipation will certainly cause the breather to decay.[3,6] More drastically, it could annihilate the breather. Topological stability arguments do not forbid annihilation. In addition, an asymptotic calculation indicates annihilation. The argument is as follows. A small-amplitude sine-Gordon breather reduces to a nonlinear Schrödinger soliton. This asymptotic reduction, when applied to the perturbed equation (2.3), yields a nonlinear Schrödinger equation for the amplitude,

$$2iA_\tau=A_{XX}+\frac{e^{-\tau}}{2}AA^*A\ .$$

The breather initial conditions (2.4) reduce to

$$A(X,\tau=0)=2\,\mathrm{sech}X\ .$$

Here, $u\simeq 2\epsilon Ae^{-\tau/2}\cos t$, $X=\epsilon x$, $\tau=\epsilon^2 t$. For $\tau\simeq 0$, this nonlinear Schrödinger equation supports a soliton; for larger τ it reduces to the linear Schrödinger equation and the soliton disperses into a packet of radiation. The numerical experiment will confirm these expectations that the breather will be annihilated.

The numerical experiment will measure both the spatial configuration $U(t)$,

$$U(t)=\{\,u(x,t),u_t(x,t)\mid \forall x\,\}\ , \tag{2.5}$$

and the spectral configuration $\hat{U}(t)$. We close this preliminary section with a brief definition of the spectral configuration. For more details, we refer to Refs. 6 and 7.

The integration of the sine-Gordon equation (2.1) is accomplished through the auxillary linear problem

$$\left[\begin{bmatrix}0 & -1\\ 1 & 0\end{bmatrix}\frac{d}{dx}+\frac{iw}{4}\begin{bmatrix}0 & 1\\ 1 & 0\end{bmatrix}+\frac{1}{16\lambda}\begin{bmatrix}e^{iu} & 0\\ 0 & e^{-iu}\end{bmatrix}\right]\vec{f}=\lambda\vec{f}\ . \tag{2.6}$$

Here $u(x,t)$ and $w(x,t)\equiv u_x+u_t$ are the "potentials" and λ denotes the eigenvalue parameter. Using this linear problem (2.6), one transforms from the spatial configuration $U(t)$ (functions of x) to the *equivalent* spectral configuration $\hat{U}(t)$ (functions of the spectral parameter λ).

The actual definition of the spectral configuration $\hat{U}$ begins with the spectrum of the linear problem (2.6). Its eigenvalues $\{\lambda_j\}$ live in the upper half λ plane and correspond to solitons in the wave $u(x,t)$; the real λ axis is continuous spectrum and is related to radiation in $u(x,t)$. Thus, the spectral configuration is

$$\hat{U}=\{\ \lambda_j,m_j\ \text{ for } j=1,2,\ldots,N;r(\lambda)\forall\lambda\epsilon R\}\ , \tag{2.7}$$

where λ_j denotes the eigenvalues and m_j denotes a normalization of the bound-state eigenfunctions. The function $r(\lambda)$ can be interpreted as the density of radiation at wavelength near $\kappa(\lambda)=2k(\lambda)$,

$$k(\lambda)=\lambda-\frac{1}{16\lambda}\ . \tag{2.8}$$

$r(\lambda)$ is defined as follows: fix an eigenfunction $\vec{f}(x,t;\lambda)$ by the asymptotic behavior as $x\to+\infty$,

$$f(x,t;\lambda)\simeq\begin{bmatrix}1\\ i\end{bmatrix}e^{ik(\lambda)x},\quad x\gg 0\ .$$

Then its behavior as $x\to-\infty$ defines the coefficient $a(\lambda)$ and $b(\lambda)$:

$$f(x,t;\lambda)\simeq a(\lambda)\begin{bmatrix}1\\ i\end{bmatrix}e^{+ik(\lambda)x}+b(\lambda)\begin{bmatrix}1\\ -i\end{bmatrix}e^{-ik(\lambda)x},$$

$$x\ll 0\ .$$

$r(\lambda)$ is then defined by the ratio

$$r(\lambda)\equiv\frac{b(\lambda)}{a(\lambda)}\ . \tag{2.9}$$

Several points should be emphasized. (i) $r(\lambda)$ is a (nonlinear) measurement of the density of nonlinear radiation at wave number near $\kappa(\lambda)=2(\lambda-1/16\lambda)$. (ii) Under perfect sine-Gordon flow, the radiation density $|r(\lambda)|$ and the eigenvalues λ_j are constant in time. (iii) The spectral configuration of the breather $u^{(B)}$ is given by

$$\hat{U}^{(B)}=\{\ \lambda_1=\tfrac{1}{4}e^{i\nu},\lambda_2=-\tfrac{1}{4}e^{-i\nu},m_1,m_2;\ r(\lambda)=0\}\ .$$

The breather (2.2) has two bound states, on a circle of radius $\frac{1}{4}$ in the upper half λ plane, whose positions are fixed by the parameter ν (Fig. 2). As the breather amplitude (4ν) decreases, the two eigenvalues approach the real axis at $\lambda=\pm\frac{1}{4}$. The breather $\hat{U}^{(B)}$ has no radiation component since $r(\lambda)=0$.

III. NUMERICAL EXPERIMENT

A. Spatial configuration

We solve numerically the sine-Gordon equation under dissipation using breather initial data, Eqs. (2.3) and (2.4). Typical spatial profiles are displayed in Fig. 3 for $x\geq 0$. The dissipation parameter is $\epsilon=0.1$ and the initial frequency parameter is $\nu=20°$. These profiles are plotted at the unit of time nearest the maximum and minimum values of v in each period.

Since dissipation is present, the wave is no longer periodic in time. However, since the dissipation is weak ($0<\epsilon=0.1\ll 1$), the wave may be

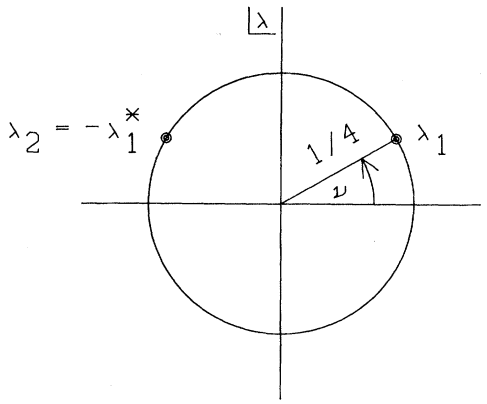

FIG. 2. Location of the zeros (λ_1,λ_2) of $a(\lambda)$ for a pure breather at rest in the laboratory frame.

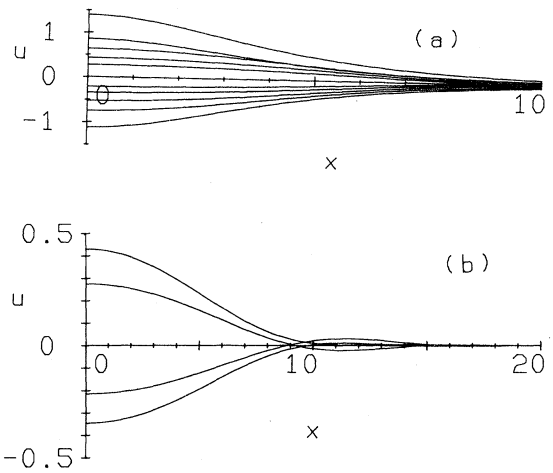

FIG. 3. Solution of the perturbed equation $u(x,t)$ at various integral times which are closest to the maximum and minimum excursions. (a) From the top curve to the x axis, $t=0,6,13,19,25$ and from the bottom curve to the x axis, $t=3,10,16,22$. (b) $t=19,\ 22,25,28$ with expanded u axis and contracted x axis to show the oscillations which are building up as t increases.

viewed as nearly periodic with slowly modulating period. We compute this period as twice the time between successive zeros of $u(x=0,t)$ and summarize the results in Table I. (The initial period is calculated as four times the time of the first zero crossing.) Notice that the period decreases from 6.91 for t between 0 and 1.6 to a value of 6.24 ($<2\pi=6.28$) by $t=18$. At this time the amplitude, which initially was 1.4, is still ~ 0.5. A perfect breather has period $2\pi/\cos\nu=(6.69>2\pi)$ and amplitude 4ν. Thus, had the wave decayed as a pure breather, it would have had no amplitude when the period reached $2\pi=6.28$. As shown in Fig. 3 there is a substantial amount of wave left at this time.

TABLE I. Period of $u(x=0,t)$ calculated from each zero crossing.

Times	Period
0–1.6	6.91
1.6–5	6.48
5–8	6.36
8–11.2	6.29
11.2–14.2	6.26
14.2–17.7	6.24
Period remains 6.24 for times of 17.7–36.3	

At later times, the wave which remains has a nearly constant period just slightly *less than* 2π. The residual radiation is primarily long-wavelength plasma radiation which continues to decay because of dissipation and spreads in space due to dispersion.

In summary, the numerically generated spatial configuration shows that the breather does not decay as a pure-breather waveform. Rather, as it decays, it generates substantial plasma radiation and by a time of 16 the breather seems to have entirely disappeared and only plasma radiation remains.

B. Numerical evaluation of the spectral representation

Now we consider the spectral representation for the numerical experiment just described. In particular, we interpret

$$|r(k,t)| = \left|\frac{b(k,t)}{a(k,t)}\right| = \frac{|b(k,t)|}{[1-|b(k,t)|^2]^{1/2}} \tag{3.1}$$

as the density of radiation at wave number $\kappa(\lambda)=2[\lambda-1/(16\lambda)]$ at time t.

Initially, the perfect breather has a spectral representation given by

$$a(k)=\frac{k-0.5i\sin\nu}{k+0.5i\sin\nu}, \qquad b(k)=0\ . \tag{3.2}$$

As dissipation causes the breather to decay the radiation density $|r|$ increases from zero and, as we will show later in this section, ν decreases through 0. Numerical values for $|b(k,t)|$ are plotted in Fig. 4. We only display $k\geq 0$ since $|b|$ is even in k.

From Fig. 4 it can be seen that $|r(k,t)|$ initially increases from 0, goes to infinity for $t\approx 14$ (as $|b|\to 1$ and so $|a|\to 0$), and finally decays back to zero because of the effect of dissipation. Note that $|r|$ reaches its peak at about the same time as the period of the waveform passes through 2π (see Table II) and that $|r|$ is certainly not of order ϵ for $t\geq 2$. The most important feature of the radiation density is its *sharp peaking about* $k=0$. For all times $t\in(0,30)$ the density is practically zero beyond $k=0.5$ with a half-width $k_{1/2}\approx 0.3$. Plasma radiation ($k=0$) is certainly the predominant mode of radiation which is excited as the

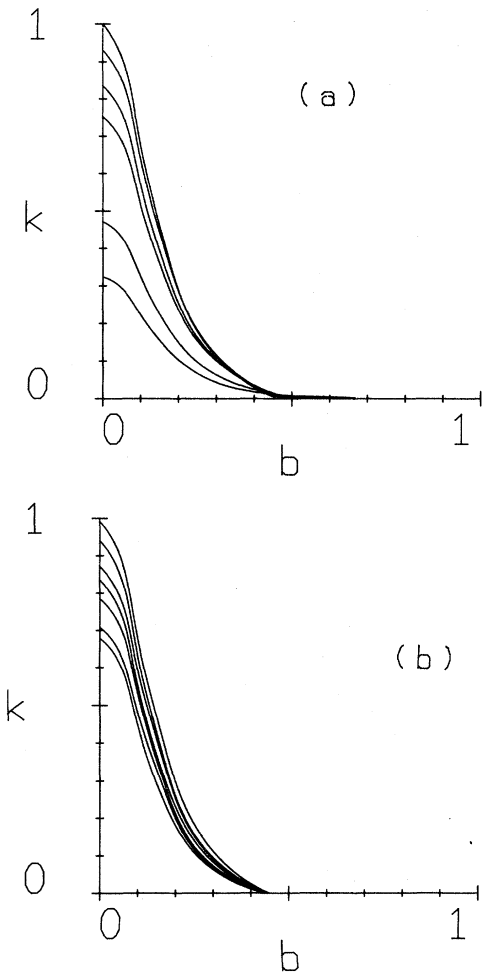

FIG. 4. $|b(k,t)|$ at various times. (a) From the k axis to the top curve, $t=0$ (k axis), 2,4,6,8,10,14 (12 is nearly indistinguishable from 14). (b) From the top curve to the k axis, $t=16$ (18 is nearly indistinguishable from 16), 20,22,24,26,28,30.

breather decays.

To show that the breather pole of r (zero of a) actually crosses into the lower half plane, we have plotted ν versus time in Fig. 5. ν was calculated by solving the linear problem, Eq. (2.6), for $a(k)$ and $b(k)$ with various complex k and then interpolating to find where $a=0$. Notice that the zero of a crosses the real axis at $t\approx 15$, which is when the period decreases past 2π and the radiation $r(\lambda)$ reaches its peak.

We emphasize that these numerical experiments measure the population of the nonlinear modes of the sine-Gordon equation. They establish that, for $t>15$ the wave no longer contains the breather. In Sec. IV, we discuss two methods for analyzing the (nonlinear) radiation density.

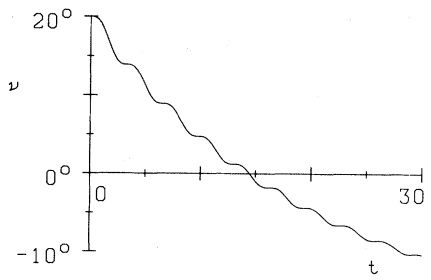

FIG. 5. Location of the zero of a moving down from $\nu=20°$, calculated numerically from Eq. (2.6) every 0.25 units of time.

IV. ANALYSIS OF THE SPECTRAL NUMERICAL DATA

Consider $|b(k,t)|$ depicted in Fig. 4. For times $t\in(0,30)$ $|b(k,t)|$ appears as a slowly varying sech profile,

$$|b(k,t)| = \gamma(t)\,\mathrm{sech}[\delta(t)k]\,. \tag{4.1}$$

At each time t, we use two points, $\lambda=0.25$ ($k=0$) and $\lambda=0.4$ ($k=0.243\,75$), to determine these parameters and then consider the accuracy of the sech representation, (4.1) at other values of k. The values of $\gamma(t)$ and $\delta(t)$ are listed in Table II and the accuracy of the sech fit is listed in Table III. For $0\le k\le 0.25$ this sech fit is accurate to within 3% for $0\le t\le 14$ and 8% for $18\le t\le 30$. This striking accuracy seems very suggestive for analytical descriptions of the radiation.

Finally, we investigate the possibility of representing the radiation in terms of resonances in the spectral representation, that is, in terms of poles (and their residues) of $r(\lambda)$ in the lower half λ plane. This approach is consistent with our numerical study, which shows breather annihilation takes place by the breather poles crossing the real

TABLE II. Coefficients of the sech representation for $|b(k,t)|$ [$\approx\gamma\,\mathrm{sech}(\delta k)$], where the coefficients are calculated by requiring equality at $k=0$ and 0.243 75.

$t=0$	$\gamma=0$	
$t=2$	$\gamma=0.322$	$\delta=9.11$
$t=6$	$\gamma=0.751$	$\delta=9.14$
$t=10$	$\gamma=0.929$	$\delta=9.31$
$t=14$	$\gamma=0.998$	$\delta=9.68$
$t=18$	$\gamma=0.963$	$\delta=9.67$
$t=22$	$\gamma=0.870$	$\delta=9.79$
$t=26$	$\gamma=0.783$	$\delta=10.20$
$t=30$	$\gamma=0.677$	$\delta=10.17$

TABLE III. Comparison of $|b(k,t)|$ calculated numerically from Eq. (2.6); the sech representation with coefficients given in Table II; the $N=1$ and the $N=2$ rational-function approximations.

k	Numerical value	sech	$N=1$	$N=2$
		$t=2$		
0	0.3220	0.3220	0.3220	0.3220
0.0385	0.3030	0.3031	0.2950	0.3024
0.0916	0.2346	0.2351	0.2121	0.2325
0.1714	0.1290	0.1293	0.1145	0.1269
0.2437	0.0690	0.0690	0.0690	0.0690
0.3750	0.0213	0.0211	0.0333	0.0243
0.6667	0.0032	0.0015	0.0113	0.0039
0.9375	0.0012	0.0001	0.0058	0.0012
		$t=6$		
0	0.7506	0.7506	0.7506	0.7506
0.0385	0.7064	0.7064	0.6872	0.7047
0.0916	0.5474	0.5471	0.4930	0.5410
0.1714	0.3007	0.3002	0.2655	0.2944
0.2437	0.1599	0.1599	0.1599	0.1599
0.3750	0.0470	0.0487	0.0770	0.0563
0.6667	0.0020	0.0034	0.0262	0.0091
0.9375	0.000 07	0.0003	0.0135	0.0027
		$t=10$		
0	0.9295	0.9295	0.9295	0.9295
0.0385	0.8747	0.8728	0.8473	0.8705
0.0916	0.6773	0.6703	0.5998	0.6622
0.1714	0.3688	0.3621	0.3181	0.3545
0.2437	0.1903	0.1903	0.1903	0.1903
0.3750	0.0484	0.0566	0.0912	0.0660
0.6667	0.0015	0.0038	0.0309	0.0105
0.9375	0.000 08	0.0003	0.0159	0.0031
		$t=14$		
0	0.9982	0.9982	0.9982	0.9982
0.0385	0.9379	0.9327	0.9007	0.9266
0.0916	0.7200	0.7030	0.6188	0.6927
0.1714	0.3798	0.3667	0.3174	0.3578
0.2437	0.1817	0.1817	0.1817	0.1817
0.3750	0.0442	0.0530	0.0886	0.0630
0.6667	0.0008	0.0032	0.0299	0.0098
0.9375	0.000 05	0.0002	0.0153	0.0028
		$t=18$		
0	0.9632	0.9632	0.9632	0.9632
0.0385	0.9041	0.9001	0.8693	0.8972
0.0916	0.6913	0.6787	0.5976	0.6688
0.1714	0.3642	0.3543	0.3068	0.3457
0.2437	0.1808	0.1808	0.1808	0.1808
0.3750	0.0357	0.0513	0.0857	0.0609
0.6667	0.0007	0.0031	0.0289	0.0095
0.9375	0.000 05	0.0002	0.0148	0.0027

TABLE III. (*Continued.*)

		$t=22$		
0	0.8696	0.8696	0.8696	0.8696
0.0385	0.8182	0.8113	0.7822	0.8085
0.0916	0.6177	0.6081	0.5325	0.5987
0.1714	0.3385	0.3140	0.2705	0.3059
0.2437	0.1588	0.1588	0.1588	0.1588
0.3750	0.0299	0.0443	0.0750	0.0530
0.6667	0.0006	0.0026	0.0252	0.0082
0.9375	0.000 05	0.0002	0.0129	0.0023
		$t=26$		
0	0.7833	0.7833	0.7833	0.7833
0.0385	0.7371	0.7266	0.6957	0.7235
0.0916	0.5671	0.5330	0.4572	0.5231
0.1714	0.2877	0.2648	0.2241	0.2568
0.2437	0.1296	0.1296	0.1296	0.1296
0.3750	0.0234	0.0342	0.0605	0.0419
0.6667	0.0027	0.0017	0.0202	0.0063
0.9375	0.000 03	0.0001	0.0104	0.0018
		$t=30$		
0	0.6773	0.6773	0.6773	0.6773
0.0385	0.6344	0.6285	0.6021	0.6259
0.0916	0.4778	0.4618	0.3967	0.4533
0.1714	0.2381	0.2300	0.1950	0.2231
0.2437	0.1128	0.1128	0.1128	0.1128
0.3750	0.0197	0.0229	0.0528	0.0366
0.6667	0.0004	0.0015	0.0176	0.0055
0.9375	0.000 02	0.0001	0.0090	0.0016

axis into the lower half λ plane. Presumably the approximation would permit the annihilation process to be described mathematically by a coupled system of ordinary differential equations for a few of these poles and their residues. Here, after checking that such an approximation could be an accurate description, we describe the motion of the poles as a function of time.

To obtain these resonances, we begin with the very accurate sech profile, and approximate it by a rational function

$$|b(k,t)| \simeq |b_{(N)}(k,t)| \equiv \frac{\gamma(t)}{\sum_{j=0}^{N}\{[\delta(t)k]/(2j)!\}^{2j}} . \tag{4.2}$$

The accuracy of these approximations for $N=1$ and $N=2$ is listed in Table III. Near $k=0$ both are very good, although of course neither algebraic decay agrees with the exponental decay of the sech for $k \geq 1$. ($N=2$ is certainly better than $N=1$.)

Then to make the zero-pole structure of $|b_N|$ more apparent, we write the approximations for $N=1$ and 2 in a more useful form:

$$|b_{(N)}(k,t)| = \begin{cases} \dfrac{\rho^{(1)}(t)}{k^2+[\beta^{(1)}(t)]^2}, & N=1 \\ \dfrac{\rho^{(2)}(t)}{\{k^2+[\beta_1^{(2)}(t)]^2\}\{k^2+[\beta_2^{(2)}(t)]^2\}}, & N=2 \end{cases} \tag{4.3}$$

where

$$\rho^{(1)}(t)=2\gamma(t)/\delta^2(t) ,$$

$$\beta^{(1)}(t)=\sqrt{2}/\delta(t) ,$$

and

$$\rho^{(2)}(t)=24\gamma(t)/\delta^4(t) ,$$

$$\beta_1^{(2)}(t)=(6+2\sqrt{3})^{1/2}/\delta(t) ,$$

$$\beta_2^{(2)}(t)=(6-2\sqrt{3})^{1/2}/\delta(t) .$$

From general spectral theory $a(k)$ can be constructed from $|b(k)|$ and the upper half-plane zeros of $a(k)$. We obtain

$$a(k,t)\simeq a_{(N)}(k,t)=\begin{cases}\dfrac{(k-i\alpha_1^{(1)})(k+i\alpha_2^{(1)})}{(k+i\beta^{(1)})^2}, & N=1\\ \dfrac{(k-i\alpha_1^{(2)})(k+i\alpha_2^{(2)})(k+i\alpha_3^{(2)})(k+i\alpha_4^{(2)})}{(k+i\beta_1^{(2)})^2(k+i\beta_2^{(2)})^2}, & N=2\end{cases} \tag{4.4}$$

where $\alpha_1^{(1,2)}$ is the zero of a corresponding to the breather and can be either positive ($0\le t\le\sim 15$) or negative ($t\ge\sim 15$). The rest of the α's are all positive. Recalling that $|a(\lambda)|^2+|b(\lambda)|^2=1$ for λ real (or eigenvalently for k real), we obtain the following conditions on α and β for $N=1$,

$$\alpha_1^{(1)}=\pm[(\beta^{(1)})^2-\rho^{(1)}]^{1/2},$$
$$\alpha_2^{(1)}=[(\beta^{(1)})^2+\rho^{(1)}]^{1/2} \tag{4.5}$$

and for $N=2$,

$$\alpha_1^{(2)}=\pm\left[\frac{B_1-(B_2^2+4\rho^{(2)})^{1/2}}{2}\right]^{1/2},$$
$$\alpha_2^{(2)}=\left[\frac{B_1-(B_2^2-4\rho^{(2)})^{1/2}}{2}\right]^{1/2},$$
$$\alpha_3^{(2)}=\left[\frac{B_1+(B_2^2-4\rho^{(2)})^{1/2}}{2}\right]^{1/2}, \tag{4.6}$$
$$\alpha_4^{(2)}=\left[\frac{B_1+(B_2^2+4\rho^{(2)})^{1/2}}{2}\right]^{1/2},$$

where

$$B_1=(\beta_1^{(2)})^2+(\beta_2^{(2)})^2$$

and

$$B_2=(\beta_1^{(2)})^2-(\beta_2^{(2)})^2.$$

Thus, for this problem, all of these resonance parameters are fixed by the two parameters of the sech profile, $\gamma(t)$ and $\delta(t)$.

To understand the zero-pole structure of these resonances, let us concentrate on $N=1$. At time 0 the waveform is a perfect breather with the spectral representation for a and b given by (3.2) where $\nu=20°$. This agrees with the a and b given in (4.4) if $\rho=0$ and, from (4.5),

$$\alpha_2^{(1)}(t=0)=\beta^{(1)}(t=0)$$
$$=\alpha_1^{(1)}(t=0)=0.5\sin 20°.$$

Thus a zero of order 1 and a pole of order 2 coincide at $k=-0.5i\sin 20°$ (i.e., $\nu=-20°$). At time increases the breather decay and emits radiation so $b\neq 0$ and thus $\rho\neq 0$. From (4.5) it follows that the pole and zero in the lower half plane split apart.

In Table IV we give α and β for $N=1$ and 2 corresponding to the γ's and δ's listed in Table II. To check on the accuracy of these rational functions, in Table V we compare $\alpha_1^{(1)}$ and $\alpha_1^{(2)}$ with the zero of a in Fig. 5 which was calculated numerically by solving the eigenvalue equation (2.6). Note that the zero from (2.6) and the $N=2$ zero agree quite closely for $0\le t\sim 16$, which is when the sech is a very good approximation to r (see Table III).

In Fig. 6 we plot the zeros and poles of $a(\lambda)$ for $N=2$. Since the sech profile is such a good approximation to $|r(k)|$, we would obtain better approximations to the zero and pole structure of the breather decay by using higher-degree rational functions. However, the essential details can be seen in Fig. 6. Namely, zeros and poles split apart in the lower half plane and the upper half-plane zero travels into the lower half plane. [Since u is symmetric about the x axis, a point λ, at which a zero or pole exists, either satisfies $|\lambda|=\frac{1}{4}$ or there is another zero or pole, respectively, at $1/(16\lambda^*)$.]

V. CONCLUSION

In conclusion, we emphasize a few points.

(i) This numerical experiment provides quantitative measurement of the spectral configuration dur-

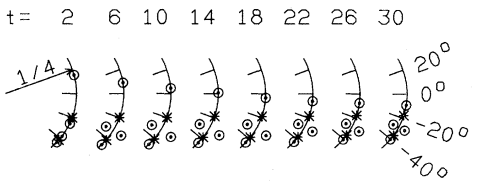

FIG. 6. Locations of the zeros (circles) and poles (asterisks) of $a(\lambda)$ for the $N=2$ rational-function approximation. (The poles are of order 2.)

TABLE IV. Locations of the zeros and poles of $a(\lambda)$ from the $N=1$ and $N=2$ rational-function approximation. (λ representation.)

	$N=1$		$N=2$	
t	Zeros	Pole	Zeros	Poles
2	(0.244, 0.052) (0.239,−0.073)	(0.242,−0.064)	(0.241, 0.067) (0.226,−0.107) (0.198,−0.153) (0.180,−0.174)	(0.235,−0.085) (0.187,−0.166)
6	(0.248, 0.032) (0.236,−0.084)	(0.242,−0.063)	(0.246, 0.039) (0.187,−0.117) (0.240,−0.150) (0.172,−0.182)	(0.235,−0.085) (0.188,−0.165)
10	(0.249, 0.016) (0.235,−0.086)	(0.242,−0.062)	(0.249, 0.020) (0.182,−0.112) (0.249,−0.154) (0.172,−0.181)	(0.236,−0.084) (0.191,−0.162)
14	(0.250, 0.002) (0.236,−0.083)	(0.243,−0.059)	(0.250, 0.003) (0.184,−0.108) (0.253,−0.148) (0.179,−0.175)	(0.237,−0.080) (0.196,−0.155)
18	(0.250,−0.011) (0.236,−0.082)	(0.243,−0.059)	(0.250,−0.014) (0.185,−0.109) (0.251,−0.148) (0.179,−0.174)	(0.237,−0.080) (0.196,−0.155)
22	(0.249,−0.021) (0.237,−0.079)	(0.243,−0.058)	(0.249,−0.026) (0.189,−0.107) (0.248,−0.134) (0.183,−0.171)	(0.237,−0.079) (0.197,−0.153)
26	(0.249,−0.025) (0.239,−0.072)	(0.244,−0.054)	(0.248,−0.032) (0.200,−0.106) (0.246,−0.133) (0.190,−0.162)	(0.238,−0.076) (0.202,−0.147)
30	(0.248,−0.031) (0.240,−0.071)	(0.244,−0.055)	(0.247,−0.040) (0.201,−0.108) (0.241,−0.130) (0.191,−0.161)	(0.238,−0.076) (0.202,−0.147)

ing the annihilation of a breather by simple dissipation. In particular, it establishes that the breather is annihilated *in finite time.* We believe this qualitative effect deserves an analytical description, which should be feasible in this simple situation.

(ii) Intuition indicates, and these measurements confirm, that long-wavelength radiation plays a fundamental role in this annihilation process. Most perturbation calculations ignore radiation *when computing the solitons's response* to perturbations and then use the soliton's response to compute the radiation which is generated. This approach will not predict annihilation in finite time, as the following simple argument shows. Let H denote the sine-Gordon Hamiltonian,

$$H(u)=\int_{-\infty}^{\infty}[\tfrac{1}{2}(u_t^2+u_x^2)+1-\cos u]dx\ .$$

If u satisfies the sine-Gordon equation with dissipation (2.3), one computes

TABLE V. Location of the zero of a moving down from $\nu=20°$, calculated numerically from (2.6) and calculated from the $N=1$ and the $N=2$ rational-function approximations.

	Zero		
t	From (2.6)	$N=1$	$N=2$
2.0	15.7°	12.1°	15.6°
4.0	13.7°	10.7°	13.5°
6.0	9.1°	7.3°	8.9°
8.0	7.3°	5.7°	7.0°
10.0	4.8°	3.8°	4.6°
12.0	1.8°	1.4°	1.7°
14.0	0.8°	0.6°	0.7°
16.0	−1.8°	−1.4°	−1.7°
18.0	−3.3°	−2.6°	−3.1°
20.0	−4.4°	−3.2°	−3.9°
22.0	−6.4°	−4.8°	−5.9°
24.0	−7.1°	−5.3°	−6.6°
26.0	−8.5°	−5.8°	−7.4°
28.0	−9.8°	−6.9°	−8.8°
30.0	−10.3°	−7.1°	−9.1°

$$\dot{H}(u)=-2\epsilon\int_{-\infty}^{\infty}\frac{u_t^2}{2}dx$$

$$=-2\epsilon H(u)+2\epsilon\int_{-\infty}^{\infty}\left[\frac{u_x^2}{2}+1-\cos u\right]dx\ .$$

Therefore,

$$\dot{H}(u)+2\epsilon H(u)\geq 0\ .$$

If, in order to compute the response of the breather parameter ν to dissipation one assumes

$$u=u^{(B)}[x,t;\nu(t)]\ ,$$

this inequality yields

$$\frac{dH(u^{(B)})}{dt}+2\epsilon H(u^{(B)})\geq 0\ .$$

Thus, the energy of the breather lies above an exponentially decaying curve and never reaches zero in finite time. Apparently, one needs radiation to "pull the breather parameter across the real axis."

(iii) There is some analytical work on the generation of a shelf as a Korteweg–de Vries soliton responds to dissipation[8,9] by a pole crossing the real axis. Perhaps these techniques would apply here.

(iv) A simple analytical description of the annihilation process needs a leading description of the wave which includes both the breather and long-wavelength radiation. The sech profile of the radiation density could be useful here.

ACKNOWLEDGMENTS

We thank H. Flaschka and E. Larsen for many helpful discussions and calculations concerning the analysis in this paper, A. Newell for useful comments concerning the numerical experiment, and W. Ferguson, Jr. for useful comments about the numerical methods. The work of D.W.M was supported in part by a National Science Foundation Grant No. MSC-7903533 and by the Department of Energy (Los Alamos Scientific Laboratory, Group T-7). The work of E.A.O. was supported in part by the Army Research Office Grant No. DAAG29-78-G0059.

APPENDIX: COMPUTER CODE

The sine-Gordon equation was solved numerically using the leap-frog method in time, i.e,

$$u_{tt}\rightarrow u(t+\Delta t)-2u(t)+u(t-\Delta t)$$

with $\Delta t=0.025$, and Fourier transform in space, i.e., $u_{xx}\rightarrow\mathcal{F}^{-1}(-k^2\mathcal{F}(u))$ with $\Delta x=0.075$. Periodic boundary conditions were used with the period being 76.8. The program was started using Euler in time with $\Delta t=0.025/2^8$ and then doubling the time step using leap-frog until $\Delta t=0.025$ was attained. All calculations were done in double precision on a DEC-10 at the University of Pittsburgh.

The calculations of $a(\lambda)$ and $b(\lambda)$ were done by solving the scattering equation (2.6) for $-l/2\leq x\leq l/2$ where $l=50.0$ and for various complex λ. The initial condition was

$$f(x=l/2;\lambda)=\begin{bmatrix}1\\ i\end{bmatrix}e^{ik(\lambda)l/2}$$

and a and b were found by solving

$$f(x=-l/2;\lambda)=a(\lambda)\begin{bmatrix}1\\ i\end{bmatrix}e^{-ik(\lambda)l/2}$$

$$+b(\lambda)\begin{bmatrix}1\\ -i\end{bmatrix}e^{ik(\lambda)l/2}\ .$$

As l increases, more of u will be contained in $[-l/2,+l/2]$ but the calculations of a and b will be less accurate due to roundoff errors (especially when the zero is in the lower half plane). As a

check on the accuracy a was calculated at $t=0$ and $\lambda=0.25e^{i\theta}$ for all integral values of θ in [0°,40°] and was found to agree with the analytical solution, Eq. (3.2), to 5 decimal places.

As a check on the accuracy of the time evolution the unperturbed sine-Gordon equation, Eq. (2.1), was run to $t=20$. At $k=0$ a changed from $(-1.000000, -0.000002)$ at $t=0$ to $(-1.000000, -0.0000006)$ at $t=20$ and b changed from (0.00693, 0.000015) to (0.000351, 0.000580). At $k=0.9375$ a changed from (0.935595, −0.353074) to (0.935594, −0.353076) and b changed from (0.000008, 0.000004) to (−0.000053, −0.000026). The analytical values of a are $(-1.0, 0.0)$ at $k=0$ and (0.935596, −0.353073) at $k=0.9375$ and $b\equiv 0.0$.

[1]A. Bishop, *Physics in One Dimension,* edited by J. Bernasconi and T. Schneider (Springer, Berlin, 1980).
[2]S. Trullinger (private communication).
[3]D. K. Kaup and A. Newell, Proc. R. Soc. (London) A 361, 413 (1978).
[4]J. Keener and D. W. McLaughlin, Phys. Rev. A 16, 777 (1977).
[5]V. I. Karpman and E. M. Maslov, Zh. Eksp. Teor. Fiz. 73, 537 (1977) [Sov. Phys.—JETP 46, 281 (1977)].
[6]See, for example, McLaughlin and Scott, Phys. Rev. A 18, 1652 (1978).
[7]L. A. Takhtadzhyan and L. D. Faddeev, Theor. Math. Fiz. (USSR) 21, 160 (1974).
[8]V. I. Karpman and E. M. Maslov, Zh. Eksp. Teor. Fiz. 75, 504 (1978) [Sov. Phys.—JETP 48, 252 (1978)].
[9]A. Newell, private communication.